Published in final edited form as:
Traffic. 2010 December ; 11(12): 1567–1578. doi:10.1111/j.1600-0854.2010.01117.x.

Drosophila Rolling Blackout Displays Lipase Domain-Dependent and Independent Endocytic Functions Downstream of Dynamin

Niranjana Vijayakrishnan, **Scott E. Phillips**, and **Kendal Broadie**
Department of Biological Sciences, Vanderbilt Brain Institute, Vanderbilt University, Nashville TN 37235-1634 USA

Abstract

Drosophila temperature-sensitive *rolling blackout* (rbo^{ts}) mutants display a total block of endocytosis in non-neuronal cells and a weaker, partial defect at neuronal synapses. RBO is an integral plasma membrane protein and is predicted to be a serine esterase. To determine if lipase activity is required for RBO function, we mutated the catalytic serine 358 to alanine in the G-X-S-X-G active site, and assayed genomic rescue of *rbo* mutant non-neuronal and neuronal phenotypes. The rbo^{S358A} mutant is unable to rescue *rbo* null 100% embryonic lethality, indicating that the lipase-domain is critical for RBO essential function. Likewise, the rbo^{S358A} mutant cannot provide any rescue of endocytic blockade in rbo^{ts} Garland cells, demonstrating that the lipase-domain is indispensable for non-neuronal endocytosis. In contrast, rbo^{ts} conditional paralysis, synaptic transmission block and synapse endocytic defects are all fully rescued by the rbo^{S358A} mutant, showing that the RBO lipase-domain is dispensable in neuronal contexts. We identified a synthetic lethal interaction between rbo^{ts} and the well-characterized dynamin GTPase conditional *shibire* (shi^{ts1}) mutant. In both non-neuronal cells and neuronal synapses, shi^{ts1};rbo^{ts} phenocopies shi^{ts1} endocytic defects, indicating that dynamin and RBO act in the same pathway, with dynamin functioning upstream of RBO. We conclude that RBO possesses both lipase-domain dependent and scaffolding functions with differential requirements in non-neuronal versus neuronal endocytosis mechanisms downstream of dynamin GTPase activity.

Keywords

shibire; serine esterase; endocytosis; synaptic vesicle; endosome; Giant Fiber circuit; neuromuscular junction; Garland cell

Introduction

The lipid composition of the plasma membrane determines its flexibility, curvature and trafficking properties. Membrane retrieval endocytosis mechanisms are critically dependent on the temporally-regulated focal accumulation of specific lipids. Numerous endocytic proteins have selective domains that recognize different membrane lipids. Pleckstrin homology (PH) and AP180 N-terminal homology/Epsin N terminal homology (ANTH/ENTH) domains bind acidic phospholipids such as phosphatidylinositol (4,5)- bisphosphate (PIP_2). PIP_2 is required for several steps in endocytic vesicle retrieval including clathrin coat nucleation, vesicle budding, scission and uncoating (1,2). The recruitment of endocytic adaptor proteins AP2 and AP180 requires PIP_2. Bar (Bin Amphyphysin RVS) domain containing proteins such as endophilin and amphyphysin also bind negatively charged

Correspondence: Kendal Broadie, PhD, Department of Biological Sciences, Vanderbilt University, VU Station B, Box 351634, Nashville, Tennessee 37235-1634 USA, Phone: (615) 936-3937, Fax: (615) 936-0129, kendal.broadie@vanderbilt.edu.

membrane lipids and facilitate membrane curvature during vesicle formation (3,4). The GTPase dynamin PH domain also binds PIP_2 (5), and PH domain mutations inhibit dynamin function to block vesicle endocytosis (6,7). Mutations that decrease brain PIP_2 levels, result in delayed endocytosis and slower vesicle recycling kinetics (2).

We previously reported the cloning and characterization of the *Drosophila* gene *rolling blackout* (*rbo*), also known as *conserved membrane protein at 44E* (*cmp44E*) and *stambhA* (*stmA*) (8,9). Null *rbo* mutants are 100% late embryonic lethal with zero escapers, whereas a conditional temperature sensitive mutant (rbo^{ts}) paralyzes within minutes at restrictive temperature and acutely blocks synaptic transmission. Conditional rbo^{ts} mutants display an activity-dependent complete loss of phospholipase C (PLC)-mediated phototransduction and consistently, at the molecular level, rapidly accumulate phosphatidylinositol-4 phosphate (PI4P) and PIP_2, and concomitantly lose diacylglycerol (DAG), within minutes after exposure to restrictive temperature (8). RBO is an integral transmembrane plasma membrane protein with significant domain homology to membrane lipases, containing the pentapeptide motif G-X-S-X-G in which the central serine (358) functions as the catalytic active site together with a histidine (H289) and an aspartate (D719), forming a serine esterase catalytic triad similar to sn-1 DAG lipase and neuropathy target esterase/*swiss cheese* (10,11). These data strongly suggest that RBO functions directly as a lipase in the PIP_2-DAG pathway. On the other hand, the yeast RBO homolog EFR3 (Pho eighty five requiring 3) is proposed to function as a scaffolding protein required for recruiting PI4P kinase, and thus only indirectly regulating plasma membrane phosphoinositide signaling (12). In the absence of yeast EFR3, cells fail to assemble the membrane kinase complex and thereby accumulate altered levels of PI4P and PIP_2 (12). These data suggest that RBO may have a critical scaffolding function completely independent of its lipase activity.

RBO is expressed in the plasma membrane of both neurons and non-neuronal cells, albeit particularly enriched in neuronal synapses. Conditional rbo^{ts} mutants demonstrate a strong temperature-dependent defect in vesicle endocytosis in both non-neuronal cells and neuronal synapses (13). Non-neuronal, endocrine Garland cells show an absolute complete endocytic block in tracer uptake assays. In contrast, neuronal synapses show a much weaker defect in styryl FM dye endocytosis, with a ~50% reduction in dye uptake (13). These data previously led us to speculate on several mechanistic hypotheses about the role of RBO relative to the *shibire* GTPase dynamin. The extremely well characterized $shibire^{ts1}$ is a dominant negative temperature-sensitive mutation that blocks the ability to pinch-off vesicles in both non-neuronal and synaptic contexts (14). We made shi^{ts1}; rbo^{ts} double mutants to determine the relative role of RBO in these processes, and to test whether RBO functions up- or down-stream of vesicle scission in both neuronal and non-neuronal endocytosis.

In the present study, we first investigate the effects of an engineered point mutation targeting the RBO predicted lipase active site. We show that in null *rbo* mutants, the rbo^{S358A} mutant protein is stable, normally expressed and localized, but provides no rescue of embryonic lethality, indicating that the RBO lipase-domain is essential. Consistently, we show that the RBO lipase-domain is completely required for vesicle endocytosis in non-neuronal cells in the TS background, again indicating that the lipase-domain is required for membrane trafficking. On the other hand, the rbo^{S358A} mutant fully rescues the TS paralytic behavior, loss of synaptic transmission and the endocytic defect at rbo^{ts} neuronal synapses, showing that the lipase-domain is not essential in neurons, presumably due to a neural-specific compensating pathway. Secondly, to investigate the RBO endocytic mechanism, we examine genetic interactions between rbo^{ts} and shi^{ts1}. We show that a synthetic lethal interaction occurs in rbo^{ts}; shi^{ts1} double mutants, indicating that they function in a common pathway required for viability. Consistently, the double mutants phenocopy the shi^{ts1} single mutant in all neuronal and non-neuronal membrane trafficking assays, indicating that shi^{ts1}

is epistatic to *rbo*^{ts1}. We therefore conclude that dynamin functions upstream of RBO in endocytosis, and that RBO has both lipase-domain and membrane scaffolding functions, which are differentially required in neurons and non-neuronal cells.

Results

The RBO lipase-domain mutant does not rescue *rbo* null embryonic lethality

Mutation of the RBO lipase-domain was generated by targeting the G-X-S-X-G predicted enzyme active site in the genomic *rbo* sequence (*rbo*S-A:GFP; Fig. 1A, top). An EGFP tag was added at the carboxyl terminus of the transgene to track expression. The tagged transgene along with native promoter and 5' regulatory sequences was cloned into the pUAST vector, and the construct was microinjected into control ^{w1118} embryos. Stably integrated genomic lines were recovered and self perpetuating stocks were generated. For ease of manipulation, a third chromosome transformant was selected over the MKRS balancer and crossed to animals bearing balanced *rbo*^{ts} and the *rbo* deficiency (Δ) (8) chromosome over CyO or CyOGFP (Fig.1A, bottom). This cross scheme produced a self perpetuating stock containing either the *rbo* null allele over balancer or homozygous *rbo*^{ts} with a single copy of the transgene over balancer. Homozygous animals bearing the transgene were late embryonic/early L1 larval lethal.

Null *rbo* mutants die as mature embryos. In order to determine if the *rbo*S-A:GFP transgene can rescue the lethality of the null condition, embryo hatching and viability was quantified (Fig. 1B). Hatching of GFP negative and positive animals was scored, and compared between animals carrying the *rbo* null allele over a CyOGFP balancer with and without a single copy if the *rbo*S-A:GFP transgene (Δ/CyOGFP; *rbo*S-A:GFP and Δ/CyOGFP, repectively). Unhatched GFP negative embryos from these intercrosses are homozygous for the *rbo* null allele. In these embryos, the robust, wide-spread GFP signal from the CyOGFP balancer is easily distinguished from the faint, spatially restricted *rbo*SA:GFP transgene signal (Fig. 2). The hatching efficiency in the *rbo* null carrying wildtype *rbo*:GFP was indistinguishable from wildtype controls (98.75% ± 1.5, n = 400; Fig. 1B). The hatching efficiency of GFP-positive embryos (CyOGFP balancer and therefore carrying the wildtype *rbo* allele) was not significantly different between Δ/CyOGFP and Δ/CyOGFP; *rbo*S-A:GFP genotypes (Δ/CyOGFP, 45.5% ± 2.64, n = 400 and Δ/CyOGFP; *rbo*S-A:GFP, 49.75% ± 1.70, n = 400). The percentage of GFP negative unhatched embryos (*rbo* null, with or without *rbo*S-A:GFP transgene) was also not significantly different between the two groups (Δ/Δ, 47.6% ± 3.14, Δ/Δ; *rbo*S-A:GFP, 48.6%± 1.51). Therefore, the *rbo*S-A:GFP transgene in the *rbo* null background is unable to provide any rescue of the lethality caused by loss of RBO (Fig. 1B).

To determine if the *rbo*S-A:GFP transgene is stably expressed with normal localization, transgene expression driven by the native *rbo* promoter was examined by Western blot and confocal imaging (Fig. 2). Wildtype *rbo*:GFP, *rbo*S-A:GFP and wildtype Oregon-R (OR) heads were homogenized in Laemmli sample buffer and separated by electrophoresis on a 4–20% SDS-PAGE gel (Fig. 2A). When normalized to α-tubulin levels, *rbo*S-A:GFP transgene expression was indistinguishable from wildtype *rbo*:GFP (0.24 ± 0.02 and 0.29 ± 0.04, respectively). Wildtype *rbo*:GFP expression can be detected in the embryonic ventral nerve cord (VNC) as early as stage 9 (8). The protein is rapidly restricted to the synaptic neuropil in the ladder-like array typical of synaptic markers (Fig. 2B). In order to compare mutant *rbo*S-A:GFP expression to wildtype *rbo*:GFP expression, age-matched embryos bearing a single copy of either the mutant transgene or the wildtype transgene driven by the same endogenous native promoter were examined. Expression of the mutant protein was indistinguishable from the wildtype protein (Fig. 2B). Finally, subcellular protein expression was examined at the larval neuromuscular junction (NMJ), double-labeled with the

presynaptic marker cysteine-string protein (CSP). The fluorescence level and synaptic bouton distribution of *rbo*S-A:GFP was indistinguishable from wildtype *rbo*:GFP (Fig. 2C). These cumulative data show that *rbo*S-A:GFP is stable and normally localized *in vivo*. Importantly, this lipase-domain mutant protein is unable to provide the essential wildtype RBO function required for embryonic viability.

RBO lipase-domain is required for Garland cell plasma membrane endocytosis

Drosophila Garland cells (or "wreath" cells) encircle the anterior end of the oesophagous above the proventriculous (15–17), and act as nephrocytes analogous to the kidneys of higher animals. These cells are highly specialized for clathrin-mediated fluid phase endocytic uptake from the haemolymph. Mainly due to their large size and ease of visualization, these cells have been used extensively as a model system to study mechanistic aspects of endocytic trafficking (15,16,18). We previously showed that RBO is expressed in the plasma membrane of Garland cells, and that *rbo*^{ts} mutants show a temperature-dependent complete block in texas-red avidin tracer uptake (13). The Garland cell plasma membrane is riddled with deep invaginations, called labyrinthine channels, from which vesicles are pinched off by clathrin-mediated endocytosis (CME) (18). Typically these channels are short because the endocytic pinch-off rate matches the membrane re-insertion rate (16). However, in *rbo*^{ts} mutants at restrictive temperature, labyrinthine channels become greatly elongated and engorged, similar to defects seen in other endocytic mutants, due to a failure to endocytic pinch-off while membrane insertion continues (16).

In order to determine whether the lipase domain is required for RBO endocytic function, we performed tracer uptake assays in Garland cells isolated from *rbo*^{ts} animals expressing *rbo*S-A:GFP (Fig. 3). Following TR-avidin uptake of 2 minutes at permissive 25°C, both control (OR) cells and *rbo*S-A:GFP cells take up tracer into discrete puncta/vesicles within the cell (Fig. 3A, left column; plasma membrane and internalized vesicles shown with white arrowheads and arrows, respectively). At permissive temperature, the total number of endocytosed vesicles in control and *rbo*S-A:GFP is indistinguishable (OR, 47.42 ± 2.26; *rbo*S-A:GFP, 41.67 ± 2.93; Fig. 3B). At the restrictive 37°C, however, while wildtype cells continue to display robust tracer uptake (OR, 53.11 ± 1.39; Fig. 3A,B), no tracer-positive vesicles occur in *rbo*S-A:GFP cells (*rbo*S-A:GFP, 0.62 ±0.59, $p<0.001$; Fig. 3A,B). These data show that there is a complete block in Garland cell endocytosis in *rbo*^{ts}; *rbo*S-A:GFP animals, just as complete as in the *rbo*ts mutant (13). Thus, the *rbo*S-A:GFP transgene is unable to provide a rescue of function. The fact that the endocytic block continues when the *rbo*S-A:GFP transgene is introduced indicates that the RBO lipase-domain is fully required for membrane trafficking in these cells.

RBO lipase-domain mutant rescues paralysis and synaptic function defects

Conditional *rbo*^{ts} mutants display conditional temperature-sensitive paralysis (9). In adult animals, there is a reversible loss of synaptic transmission excitatory junction potentials (EJPs) on dorsal longitudinal muscles (DLMs) following motor nerve stimulation, suggesting that paralysis is due to a neurotransmission defect (9). The NMJ is a well studied model for assays of synaptic function. Muscles have a stereotypical pattern of innervation, and are amenable to optical imagining assays to study vesicle exo/endocytosis cycling (19). Previously, we showed that *rbo*^{ts} mutants show a temperature-dependent defect in depolarization dependent lipophilic styryl dye FM1–43 uptake into 3rd instar larval NMJs, indicative of a defect in plasma membrane endocytosis (13). This defect is completely rescued by a single copy of a wildtype *rbo* transgene driven by its endogenous promoter (13).

We first tested whether introduction of the *rbo*S-A:GFP transgene rescues *rbo*^{ts} paralysis (19,20). Four genotypes were analyzed, control (OR), *rbo*^{ts} alone (conditional mutant over deficiency; *rbo*^{ts}/Δ), *rbo*:GFP/y; *rbo*^{ts}/Δ and *rbo*^{ts}/Δ; *rbo*S-A:GFP/MKRS; (Table 1). All animals were raised together at 25°C, and then acutely shifted to 35, 37 or 39°C by immersion in a water bath (see Supplemental Movie S1). At the 25°C permissive temperature, all genotypes were active and indistinguishable from each other in their behaviors. At the 37°C restrictive temperature, control animals remain active, and indeed have a noticeable increase in activity levels. In contrast, 100% of *rbo*^{ts}/Δ animals paralyze within 5 minutes after a shift to 37°C (Table 1; Movie S1). Mutant animals show no detectable movement when paralyzed, but fully recover movement after 5 minutes at 25°C. Under identical conditions, *rbo*S-A:GFP expressing *rbo*^{ts}/Δ animals are still able to behave similar to control OR and *rbo*:GFP/y; *rbo*^{ts}/Δ animals. The movement behavior of the lipase-domain mutant animals is indistinguishable from controls. Decreasing and increasing the temperature to 35°C and 39°C causes a concomitant change in the time for *rbo*^{ts}/Δ animals to paralyze, while the *rbo*:GFP; *rbo*^{ts}/Δ and *rbo*S-A:GFP; *rbo*^{ts}/Δ animals remain fully active for all timepoints analyzed (Table 1). Thus, the presence of the *rbo*S-A lipase domain mutant protein is able to fully rescue the conditional *rbo* paralytic phenotype.

We next tested whether the *rbo*S-A:GFP mutant transgene could rescue the *rbo*ts synaptic transmission blockade at 37°C (9). The adult giant fiber (GF) circuit is a well-characterized pathway that descends from brain giant neurons via the GF onto thoracic ganglion motor neurons and then NMJ transmission to muscle (21,22). In these trials, the brain was electrically stimulated with extracellular tungsten electrodes while intracellular EJP recordings were made from thoracic DLM muscle (Fig. 4). At the permissive temperature (30°C), evoked EJP amplitudes in *rbo*^{ts} mutants are indistinguishable from wildtype controls (*rbo*^{ts}/Δ, 48.3 ± 2.5 mV; OR, 42.6 ± 2.0 mV; Fig. 4B). In *rbo*^{ts}/Δ animals expressing either the *rbo*:GFP or the *rbo*S-A:GFP transgene, similar EJP amplitudes were recorded at the permissive temperature (*rbo*:GFP, 47.3 ± 7.1 mV; *rbo*S-A:GFP, 48.9 ± 1.2 mV). In sharp contrast, after acute shift to restrictive temperature (37°C), evoked EJPs in *rbo*^{ts} mutants are effectively abolished ($p<0.001$), whereas OR control EJP amplitudes remain robust (*rbo*^{ts}/Δ, 1.4 ± 1.2mV; OR, 43.1 ± 6.7 mV; Fig. 4A,B). Importantly, expression of either *rbo*:GFP or *rbo*S-A:GFP in *rbo*^{ts} animals was equally effective in completely restoring the EJP response to wildtype levels (*rbo*:GFP, 51.8 ± 6.3 mV; *rbo*S-A:GFP, 48.4 ± 4.6 mV; Fig. 4A,B). We conclude that the *rbo*S-A lipase domain mutant protein fully rescues *rbo*^{ts} conditional loss of synaptic transmission.

We finally tested whether the *rbo*S-A:GFP mutant transgene could rescue the *rbo*^{ts} endocytic trafficking defects at the NMJ (13). FM1–43 dye uptake assays do not work at the adult DLM NMJ synapse, so as previously we employed the accessible larval 3rd instar NMJ (Fig. 5). Dye was loaded for 2 minutes in 60 mM [K^+] depolarizing saline following 10 minutes of incubation in 0 Ca^{2+} saline at the 37°C restrictive temperature (Fig. 5A). As shown previously, *rbo*^{ts} mutants show a highly significant decrease ($p<0.001$) in dye loading compared to wildtype controls (OR, 78.24 ± 4.07; *rbo*ts, 35.59 ± 3.11; Fig. 5B). In contrast, FM1–43 dye loading in the presence of the *rbo*S-A:GFP transgene was not significantly different from control ($p=0.285$). The *rbo*S-A:GFP mutant protein was able to fully rescue the *rbo*^{ts} endocytic defect (*rbo*^{ts}; *rbo*S-A, 71.74 ± 3.99; Fig. 5B, right). These data suggest that the RBO lipase-domain is not required for maintained movement, neural circuit function or synapse endocytic function. We conclude that there is a clear differential requirement for the RBO lipase-domain in non-neuronal versus neuronal endocytosis mechanisms, with this domain being required only in the non-neuronal context.

Dynamin is epistatic to RBO in synaptic endocytosis

The GTPase dynamin is one of the best studied endocytic proteins, and is known to be required for all forms of vesicle endocytosis at the *Drosophila* NMJ (14,23–25). The temperature sensitive *shibire*^{ts1} (*shi*^{ts1}) mutation was instrumental in establishing the dynamin "pinchase" role in synaptic vesicle endocytosis (14,15). There is extensive evidence to document the defective synaptic vesicle cycling in these mutants (15,26). Exposure to restrictive temperature leads to a loss of FM1–43 dye loading in synaptic vesicles indicative of an endocytosis blockade (27). Upon return to permissive temperature, recycling resumes in *shi*^{ts1} mutants (28,29). We therefore wished to map RBO function relative to this well-established requirement.

To determine if RBO acts in a dynamin dependent or independent mechanism, we set forth to make *shi*^{ts1}; *rbo*^{ts} double homozygous mutants. However, even when reared at 16–18°C, this combination produces synthetic lethality in double homozygous animals. No double homozygous female third instar larvae could be recovered, indicating that lethality occurs at the second instar stage or earlier. In contrast, *shi*^{ts1}/y; *rbo*^{ts}/Δ males can be recovered as third instars at a very low frequency at 16°C, before they also die at an early pupal stage. All adult males recovered contain balancer/y and females have either one or two copies of balancer chromosome with wildtype *shibire*. These data reveal a strong synthetic lethality between *shi*^{ts1} and *rbo*^{ts}, indicating that both work in the same essential pathway.

In assays for endocytosis at the larval NMJ, *shi*^{ts1}; *rbo*^{ts} animals were maintained in a hemizygous condition by maintaining *shi*ts1 over an FM7GFP balancer. The *shi*^{ts1}/y; *rbo*^{ts}/Δ (non-GFP males) and *shi*^{ts1}/y mutants were selected for FM1–43 dye loading experiments (Fig. 6). To test whether the presence of the *rbo*^{ts} mutation significantly exacerbates dye loading phenotypes in the *shi*^{ts1} background, FM 1–43 dye was loaded with 60 mM [K+] depolarizing saline for a prolonged period (4 minutes) at 18°C (Fig. 6A). Under these conditions, both *shi*^{ts1}/y and *shi*^{ts1}/y; *rbo*^{ts}/Δ mutants showed strikingly decreased loading compared to control (OR, 106.63 ±10.23; *shi*^{ts1}/y, 64.695 ± 7.59; *shi*^{ts1}/y; *rbo*^{ts}/Δ 53.53 ± 5.46; Fig. 6B). Both mutant genotypes were very significantly impaired relative to control ($p=0.009$ and $p=0.0004$, respectively), but were not significantly different from each other ($p=0.258$). Since the endocytic defect in *shi*^{ts1}/y is not worsened in *shi*^{ts1}/y; *rbo*^{ts}/Δ double mutants, these data indicate that RBO acts in a dynamin-dependent pathway, downstream of dynamin at the NMJ. In order to determine if this requirement is also present in non-neuronal cells, we next analyzed Garland cells membrane trafficking in double mutants.

Dynamin is epistatic to RBO in non-neuronal endocytosis

Garland cell endocytosis is also well studied in *shi*^{ts1} mutants (16). These cells are attractive because of endogenous high rates of endocytic uptake and the large cell/vesicle size that facilitates visualization. Previous analyses of *shi*^{ts1} Garland cells has revealed a doubling of surface area due to endocytic blockade, with elongation of the labyrinthine channels (15,16). Furthermore, *shi*^{ts1} Garland cells display a block in the uptake of endocytosis tracers at restrictive temperature, and the appearance of arrested coated pits but loss of coated vesicles, indicative of a block at the pinching-off stage (13,15). Given the striking differential requirements for the RBO lipase-domain between neuronal synapses and Garland cells, we wished to also map RBO function relative to this well-established dynamin requirement.

We performed Garland cell Texas-red avidin uptake assays on *shi*^{ts1}/y and *shi*^{ts1}/y; *rbo*^{ts}/Δ double mutants (Fig. 7). Garland cells were dissected and the tracer applied for 5 minutes to label internalized vesicles at a range of temperatures (Fig. 7A). No detectable tracer internalization occurred at 29°C in *shi*^{ts1} mutants. Therefore, 18°C was used as 1) this temperature reveals the synthetic lethal interaction between *shi*^{ts1} and *rbo*^{ts}, and 2) reduced

but easily detectable vesicle endocytosis persists in *shi*^{ts1} alone at this temperature (Fig. 7A). Thus, this condition maximized chances of detecting an interaction between *shi*^{ts1} and *rbo*^{ts}. The total number of internalized vesicles were counted and compared between genotypes (Fig. 7B). We found reduced rates of vesicle endocytosis in both *shi*^{ts1}/y and *shi*^{ts1}/y; *rbo*^{ts}/Δ compared to the wildtype control (OR, 47.94 ± 3.95; *shi*^{ts1}/y, 31.267 ± 4.57; *shi*^{ts1}/y; *rbo*^{ts}/Δ, 32.23 ± 5.05; Fig. 7A,B). Both mutant genotypes showed significant loss of endocystosis compared to control (p=0.04 for both), but there was no significant difference between *shi*^{ts1}/y and the *shi*^{ts1}/y; *rbo*^{ts}/Δ double mutant (p=0.80). These data indicate that RBO is acting in a dynamin-dependent pathway, downstream of dynamin, to facilitate endocytosis in Garland cells similar to the mechanism at neuronal synapses.

Endocytic proteins Eps15 and Stoned do not alter *rbo*^{ts} paralysis

The combination of *rbo*ts and *shi*ts1 results in synthetic lethality. No *shi*^{ts1}; *rbo*^{ts} double mutant adult animals can be recovered, and only rare larval escapers appear at low temperature (16–18°C). Other endocytic mutants similarly display synthetic lethality with *shi*^{ts1}, including *stoned* and *eps15* (30,31). The *stoned* locus encodes two distinct proteins, stoned A (STNA) and stoned B (STNB), which are both expressed at presynaptic NMJ terminals, and FM1–43 dye uptake assays clearly demonstrate a *stoned* requirement in plasma membrane endocytosis (19,32). Similarly, *eps15* null mutants exhibit decreased synaptic vesicle endocytosis and severe reductions in dynamin protein levels at the NMJ (33). Interestingly, *eps15* also shows a synthetic lethal interaction with *stoned* and, at the protein level, can be immunoprecipitated with dynamin and STNB antibodies (30). The mammalian STNB homolog, stonin 2, has also been reported to bind EPS15 (34).

Based on these functional and genetic interactions, we wished to test for synthetic interactions between *rbo*^{ts} and loss of function alleles of both *eps15* and *stoned*. We made transheterozygote animals with *rbo*^{ts}/Δ and the embryonic lethal STNA allele, *stn*$^{13–120}$ (*stn*$^{13–120}$/FM7; *rbo*^{ts}/Δ), embryonic lethal STNB allele, *stn*^{PH1}(*stn*^{PH1}/FM7; *rbo*^{ts}/Δ), or pharate adult lethal *eps15*^{Δ29} allele (*eps15*^{Δ29}, *rbo*^{ts}/Δ). None of these combinations showed a synthetic lethal interaction. Furthermore, introduction of *stn*$^{13–120}$, *stn*^{PH1} or *eps15*^{Δ29} alleles into *rbo*^{ts}/Δ animals did not cause detectable behaviorial effects at permissive rearing temperatures. Therefore, all mutant combinations were incubated at a range of temperatures (35–39°C) and analyzed for temperature-dependent paralysis (Supplemental Movie S2). At these *rbo*^{ts} restrictive temperatures, the double mutants did not alter the time course of *rbo*^{ts}/Δ paralysis (Table 2). Thus, *rbo* shows clear interactions with *shi*, but not with these other defined components of the endocytic cascade.

Discussion

A growing body of evidence suggests that lipid-modifying enzymes play vital roles in endocytic processes (35–38). In this context, we discovered *Drosophila* RBO to be an integral plasma membrane protein and potential lipase (8,9), which we initially described as homologous to sn-1 DAG lipase (8,10). Recently, however, a *Drosophila* homolog of sn-1 DAG lipase, inactivation-no-after-potential E (INAE), has been cloned and shown to hydrolyze DAG at the sn1 position (39). Thus, the RBO lipolytic function came into question. Mechanistically, we have shown RBO plays an essential role in endocytic trafficking in non-neuronal cells, and a weaker, facilitory role in neuronal synapses (13). In order to test the hypothesis that the lipase-domain of RBO plays a critical role in endocytosis, we therefore generated a point mutation in the predicted catalytic active site of the RBO lipase-domain (11,40). Since our attempts to characterize the enzymatic activity of heterologously expressed RBO protein were unsuccessful (41), the genetic disruption of the catalytic active *rbo*^{S358A} provides the best possible alternate method to elucidate of the *in vivo* importance of the RBO lipase-domain.

rbo is an essential gene required for cell viability (42), and lack of wildtype *rbo* causes completely penetrant embryonic lethality. Likewise, the transgene with the *rbo*^{S358A} point mutation by itself is 100% lethal, showing that the mutation alters an essential function of the protein. This result indicates the RBO lipase-domain has an essential function. Importantly, the TS mutant RBO can rescue the lethal phenotype in *rbo* null embryos, while conferring conditional paralysis and defects in cellular endocytosis (8,9,13). These data show that the TS mutant allele contains sufficient RBO activity to provide essential function. Nevertheless, *rbo*^{ts} mutants carrying the *rbo*^{S358A} point mutation still show a complete block of non-neuronal endocytosis, again demonstrating an essential lipase-domain requirement. On the other hand, these animals do not display any defects at the NMJ synapse and, consistently, do not paralyze. In this context, RBO may function as a dimer/oligomer such that the functionally intact TS site in the *rbo*S-A:GFP transgene can come together with the intact Serine 358 site to provide rescue of function. Such intragenic suppression provides a powerful tool to study the contributions of individual protein domains (43), with *Drosophila* examples including NSF ATPase domain mutants *comt*^{st53}/*comt*^{su1} (44) and *shi*^{ts2} with *suppresors of shibire* (*sushi*) (45).

A quite different possibility is that the RBO lipase-domain is simply not required for its endocytic role at neuronal synapses. In support of this idea, other synaptic enzymes with known activities modulate synaptic processes independent of that activity. For example, CaMKII acts both as a Ca^{2+}-dependent kinase and independently as a membrane scaffold. It mediates short-term synaptic plasticity in the hippocampus by scaffolding vesicle docking independently of its ability to phosphorylate itself or other targets (46). Consistently, the yeast RBO homolog EFR3/Ymr212c functions as an integral plasma membrane scaffold (12). Both *Drosophila* and yeast plasma membrane proteins are predicted to be 2-pass transmembrane proteins that regulate plasma membrane lipid levels, but by completely different proposed mechanisms. Yeast EFR3 functions to recruit PI4P kinase domains which, in turn, regulate membrane PI4P and PIP_2 levels (12). Importantly, the G-X-S-X-G lipase catalytic motif does not align between RBO and EFR3. Nevertheless, it is quite possible that RBO has both enzymatic and scaffolding roles at the synapse. Note that in neuronal synapses loss of RBO causes a weaker phenotype, indicating the presence of neural-specific compensatory mechanism.

To analyze a distinct mechanistic role of RBO in membrane trafficking during endocytosis, we compared the RBO requirement with the hallmark dynamin function (47,48). Dynamin functions to sever the necks of endocytosing vesicles directly by GTP hydrolysis-driven constriction and/or as a scaffold recruiting other proteins (25,49,50). The *shi*^{ts1} G273D TS mutation in the GTPase domain blocks the ability to pinch-off endocytosing vesicles (23,51,52). Coated/collared endocytic intermediates arrest in both neuronal synapses and non-neuronal Garland cells (15,28,53). Only rare *shi*^{ts1}; *rbo*^{ts} larval escapers appear at low temperature (16–18°C) and no double mutant animals survived to adulthood. We also analyzed potential effects between RBO and two other endocytic proteins, Eps15 and Stoned. Eps15 is proposed to act with DAP-160 in maintaining synaptic vesicle endocytosis by keeping high levels of dynamin and other endocytic proteins (33). Stoned-B also directly interacts with DAP-160 (32). While these synthetic interactions did not yield any effects on the paralysis of *rbo*^{ts} mutants, the synthetic lethal interaction between RBO and dynamin points to a direct interaction within the endocytic pathway.

Materials and Methods

Drosophila Stocks

All *Drosophila* stocks were maintained on standard cornmeal, agar, molasses medium in 18°C or 25°C light cycling incubators. Lipase-domain *rbo* mutants (see below) were

generated by embryonic injection of w^{1118} embryos. Red-eyed adult flies from injected embryos containing the transgene (mini white w^+ gene) were collected and crossed to a doubly balanced animals on 2nd and 3rd chromosomes (CyO and MKRS, respectively). Animals with the transgene insertion on the third chromosome were collected and crossed into *rbo*^{ts} or *rbo* deficiency (Δ) backgrounds. The *rbo*S-A:GFP transgenic line is homozygous lethal. The *shi*^{ts1} allele was kindly provided by Dr. Mani Ramaswami, University of Arizona. The *eps-15*$^{\Delta 29}$ allele (33) was obtained from the Bloomington stock center. The *rbo*^{ts} (8), *rbo*Δ (8), *stoned*^{PH1} (19) and *stoned*$^{13–120}$ (19) alleles were obtained from Broadie lab stocks. Mutant combinations containing *shi*^{ts1}, *eps15*$^{\Delta 29}$, *stoned*^{PH1}, and *stoned*$^{13–120}$ mutations were maintained in the hemizygous condition. Oregon-R (OR) was used as the wildtype control. In embryonic lethality tests, the following crosses were employed to generate the final genotype:

rbo^{ts}/CyO;+/TM6 X *rbo*$^{\Delta}$/CyOGFP:+/TM3
yields: *rbo*^{ts}/*rbo*$^{\Delta}$;TM3/TM6
+/CyO;*rbo*:GFP/TM6 X *rbo*$^{\Delta}$/CyOGFP;+/TM3
yields: *rbo*$^{\Delta}$/CyO;*rbo*:GFP/TM3
rbo$^{\Delta}$/CyO;*rbo*:GFP/TM3 X *rbo*^{ts}/*rbo*$^{\Delta}$;TM3/TM6
yields: *rbo*^{ts}/*rbo*$^{\Delta}$;*rbo*:GFP/TM6

Molecular techniques

Genomic *rbo* with the native promoter was tagged with a 3' terminal GFP sequence, and cloned into pUAST plasmid (8). The serine in position 358 was mutated to alanine in *rbo*S-A:GFP using the Quick Change Site-Directed Mutagenesis Kit (Stratagene, La Jolla, California) with forward 5'CGAAAATTATAG CTATTGCAGCGGGAGAAGCTGTCGGTCCCTCGGCCCTGG3' and reverse 5'CCAGGGCCGAGGGACC GACAGCTTCTCCCGCTGCAATAGCTATAATTTTCG3' primers and *rbo* genomic sequence as template for PCR. Clones were isolated by blue/white selection, and the presence of the mutation was verified by sequencing. The construct was injected into w^{1118} embryos and transgenic animals were produced by P-element mediated germ line transformation.

Behavioral Assays

For embryo hatching rate assays, animals of all genotypes were allowed to lay eggs in apple juice agar plates supplemented with yeast paste over a 10 hour period. After eggs were aged for 48 hours at 25°C, the number of GFP-positive and GFP-negative hatched and unhatched embyos was counted, and a percentage calculated for every 100 eggs. Adult paralysis assays were performed as described (9). Briefly, 5 animals of each genotype were placed in a pre-warmed empty plastic vial. The vials were then placed in a 37°C water bath, and time taken to paralyze determined. Animals that fell to the bottom of the vials and displayed a complete cessation of all movement were scored as paralyzed. Trials of paralyses for each genotype were repeated at least 3 times, with a fresh set of animals in each assay.

Western Blotting

10 heads from each genotype were homogenized in 50μL 1×Nupage LDS Sample Buffer (Invitrogen, Carlsbad, CA) with 50mM DTT. Debris was pelleted by centrifugation at 16,000x*g* and samples boiled for 10 minutes. 5μL of extracts representing 1 head were loaded onto a 4–12% Bis-Tris gel and electrophoresed at 200V in 1×MES buffer (Invitrogen, Carlsbad, CA). Protein was transferred to nitrocellulose in 1×Nupage Transfer Buffer (Invitrogen, Carlsbad, CA) plus 10% methanol at 100V for 1 hour. The membrane

was blocked for 1 hour in Odyssey Blocking Buffer (Li-Cor, Lincoln, NE) and probed for 12–16 hours at 4°C with the following antibodies: GFP (abcam, Cambridge, MA) 1:2000, α-Tubulin (Sigma, St Louis, MO), 1:400,000. Membranes were washed three times with buffer (25 mM Tris pH 8.0, 150 mM sodium chloride, 0.05% Ige-PAL-CA630). The secondary antibodies, anti-rabbit IgG IR800 (Rockland, Gilbertsville, PA) and anti-mouse IgG Alexa Fluor 680 (Invitrogen, Carlsbad, CA) were diluted 1:20,000 in Odyssey Blocking Buffer and applied for 1 hour at 25°C. The blot was washed three times with buffer and then scanned on the Odyssey Infrared Imaging System.

Embryo imaging

Timed egg lays were collected from apple juice agar plates with a mesh sieve. Live embryos were dechorionated in 50% bleach for 2–3 minutes, washed in water and mounted under coverslips on slides. Images were captured with a Zeiss 510 Meta confocal microscope with an argon 488nm laser used in excitation, a 505–530 bandpass filter and 40X, 1.3 oil-immersion objective. Images were collected at a single focal plane with the pinhole at 670μm. Images were assembled with Adobe Photoshop CS8.

NMJ imaging

Wandering 3rd instar larvae were dissected in 1×PBS and fixed in 4% paraformaldehyde + 4% sucrose in 1×PBS for 30 minutes at 25°C. Filleted larvae were washed three times with buffer (1×PBS, 1% BSA, 0.1% Triton X-100) for 30 minutes. Preparations were incubated with the following primary antibodies at 4°C for 12–16 hours: anti-GFP (abcam, Cambridge, MA) 1:2000 and anti-Cysteine String Protein (CSP (54)) 1:500. Secondary antibodies anti-rabbit-IgG AlexaFluor 488 and anti-mouse-IgG AlexaFluor 568 (Invitrogen, Carlsbad, CA) were diluted 1:250 and incubated for 2–3 hours at 25°C. Larvae were washed three times for 1 hour before mounting in Fluormount G (EMS) and imaging on a Zeiss Meta 510 confocal microscope. Images were assembled with AdobePhotoshop CS8.

Garland cell tracer assays

Tracer assays were performed on Garland cells as previously described (13,55). Briefly, Garland cells were dissected from wandering 3rd instars in Schneider's culture medium (Gibco) and incubated at 18°C, 25°C or 37°C as specified for each genotype. Texas red-conjugated avidin (0.2 mg/ml; Sigma Aldrich) was applied for 5 minutes (13). Imaging was done using a Zeiss LSM 510 Meta confocal microscope. Quantification of tracer uptake was done using Image J (NIH). The total number of tracer labeled vesicles inside the cell was counted for each condition. Images were assembled using Adobe photoshop CS2.

Electrophysiology

Excitatory junctional potential (EJP) recording in the adult giant fiber (GF) circuit as performed as previously described (9). Briefly, animals anesthetized on ice were mounted ventral side down with dental soft wax under a dissection microscope. A HCC-100A temperature controller (Dagan, Minneapolis, MN) was used for temperature control. The tip of a temperature probe (Series 935A temperature controller, Watlow, St. Louis, MO) was embedded in the wax adjacent to the animal. A glass reference electrode (filled with 3M KCl) was inserted into the abdomen, and tungsten stimulating electrodes (WPI, Sarasota, FL) inserted into each eye. A glass recording electrode (3M KCl) was driven through the dorsal thorax cuticle. Intracellular penetration into the muscle was monitored by a sudden potential drop of 40–60 mV. Signals were amplified by IX1 intracellular preamplifier (Dagan) and digitized at 100 kHz by Digidata 1322A (Molecular Devices, Union City, CA). Animals were stimulated at 0.5Hz and the first 10–20 responses at each temperature were

averaged. Data were collected and analyzed with pClamp software (version 9.2; Molecular Devices).

FM1–43 dye loading assays

FM1–43 dye labeling assays were performed as previously described (13,19). Briefly, wandering 3rd instar larvae were dissected in buffered, Ca^{2+}-free saline with Vetbond (3M) glue on sylgard coated coverslips. The saline contained 2 mM KCl, 120 mM NaCl, 70 mM sucrose and 3 mM HEPES at pH 7.2. Dissected preparations were incubated with FM1–43 dye (10 μM; Molecular Probes, Eugene, Oregon) applied with depolarizing 60mM high [K^+] saline (13). Temperatures and incubation times were as stated for the different genetic conditions. A 63 X, 0.95W water immersion objective on a Zeiss LSM 510 confocal microscope was used for image acquisition. Images were scanned from muscle 6/7 NMJs from segments A3/4 with mean pixel intensity was calculated for 10 boutons/NMJ and averaged across each animal (N = number of animals). Quantification was done using Image J (NIH), with average pixel intensity for the entire Z-stack 3D bouton determined. Images were assembled using Adobe photoshop CS8.

Supplementary Material

Refer to Web version on PubMed Central for supplementary material.

Acknowledgments

We are grateful to Dr. Mani Ramaswami for *Drosophila* stocks used in this study. We thank members of the Broadie lab for discussions and critical feedback. This work was supported in part by F32 NS058169 to S.P and by R01 GM54544 to K.B.

References

1. Cremona O, Di Paolo G, Wenk MR, Luthi A, Kim WT, Takei K, Daniell L, Nemoto Y, Shears SB, Flavell RA, McCormick DA, De Camilli P. Essential role of phosphoinositide metabolism in synaptic vesicle recycling. Cell. 1999; 99(2):179–188. [PubMed: 10535736]
2. Di Paolo G, Moskowitz HS, Gipson K, Wenk MR, Voronov S, Obayashi M, Flavell R, Fitzsimonds RM, Ryan TA, De Camilli P. Impaired PtdIns(4,5)P_2 synthesis in nerve terminals produces defects in synaptic vesicle trafficking. Nature. 2004; 431(7007):415–422. [PubMed: 15386003]
3. Gallop JL, Jao CC, Kent HM, Butler PJ, Evans PR, Langen R, McMahon HT. Mechanism of endophilin N-BAR domain-mediated membrane curvature. Embo J. 2006; 25(12):2898–2910. [PubMed: 16763559]
4. Peter, BJ.; Kent, HM.; Mills, IG.; Vallis, Y.; Butler, PJ.; Evans, PR.; McMahon, HT. Science. Vol. 303. New York, NY: 2004. BAR domains as sensors of membrane curvature: the amphiphysin BAR structure; p. 495-499.
5. Zheng J, Cahill SM, Lemmon MA, Fushman D, Schlessinger J, Cowburn D. Identification of the binding site for acidic phospholipids on the pH domain of dynamin: implications for stimulation of GTPase activity. J Mol Biol. 1996; 255(1):14–21. [PubMed: 8568861]
6. Lee A, Frank DW, Marks MS, Lemmon MA. Dominant-negative inhibition of receptor-mediated endocytosis by a dynamin-1 mutant with a defective pleckstrin homology domain. Curr Biol. 1999; 9(5):261–264. [PubMed: 10074457]
7. Vallis Y, Wigge P, Marks B, Evans PR, McMahon HT. Importance of the pleckstrin homology domain of dynamin in clathrin-mediated endocytosis. Curr Biol. 1999; 9(5):257–260. [PubMed: 10074456]
8. Huang FD, Matthies HJ, Speese SD, Smith MA, Broadie K. Rolling blackout, a newly identified PIP_2-DAG pathway lipase required for Drosophila phototransduction. Nat Neurosci. 2004; 7(10): 1070–1078. [PubMed: 15361878]

9. Huang FD, Woodruff E, Mohrmann R, Broadie K. Rolling blackout is required for synaptic vesicle exocytosis. J Neurosci. 2006; 26(9):2369–2379. [PubMed: 16510714]
10. Bisogno T, Howell F, Williams G, Minassi A, Cascio MG, Ligresti A, Matias I, Schiano-Moriello A, Paul P, Williams EJ, Gangadharan U, Hobbs C, DiMarzo V, Doherty P. Cloning of the first sn1-DAG lipases points to the spatial and temporal regulation of endocannabinoid signaling in the brain. The Journal of cell biology. 2003; 163(3):463–468. [PubMed: 14610053]
11. Muhlig-Versen M, da Cruz AB, Tschape JA, Moser M, Buttner R, Athenstaedt K, Glynn P, Kretzschmar D. Loss of Swiss cheese/neuropathy target esterase activity causes disruption of phosphatidylcholine homeostasis and neuronal and glial death in adult Drosophila. J Neurosci. 2005; 25(11):2865–2873. [PubMed: 15772346]
12. Baird D, Stefan C, Audhya A, Weys S, Emr SD. Assembly of the PtdIns 4-kinase Stt4 complex at the plasma membrane requires Ypp1 and Efr3. The Journal of cell biology. 2008; 183(6):1061–1074. [PubMed: 19075114]
13. Vijayakrishnan N, Woodruff EA 3rd, Broadie K. Rolling blackout is required for bulk endocytosis in non-neuronal cells and neuronal synapses. J Cell Sci. 2009; 122(Pt 1):114–125. [PubMed: 19066280]
14. Koenig JH, Ikeda K. Disappearance and reformation of synaptic vesicle membrane upon transmitter release observed under reversible blockage of membrane retrieval. J Neurosci. 1989; 9(11):3844–3860. [PubMed: 2573698]
15. Kosaka T, Ikeda K. Reversible blockage of membrane retrieval and endocytosis in the garland cell of the temperature-sensitive mutant of Drosophila melanogaster, shibirets1. The Journal of cell biology. 1983; 97(2):499–507. [PubMed: 6411734]
16. Narita K, Tsuruhara T, Koenig JH, Ikeda K. Membrane pinch-off and reinsertion observed in living cells of Drosophila. J Cell Physiol. 1989; 141(2):383–391. [PubMed: 2808544]
17. Chang HC, Newmyer SL, Hull MJ, Ebersold M, Schmid SL, Mellman I. Hsc70 is required for endocytosis and clathrin function in Drosophila. The Journal of cell biology. 2002; 159(3):477–487. [PubMed: 12427870]
18. Aggarwal SK, King RC. The ultrastructure of the wreath cells of Drosophila melanogaster larvae. Protoplasma. 1967; 63(4):343–352. [PubMed: 6081634]
19. Fergestad T, Broadie K. Interaction of stoned and synaptotagmin in synaptic vesicle endocytosis. J Neurosci. 2001; 21(4):1218–1227. [PubMed: 11160392]
20. Trotta N, Rodesch CK, Fergestad T, Broadie K. Cellular bases of activity-dependent paralysis in Drosophila stress-sensitive mutants. J Neurobiol. 2004; 60(3):328–347. [PubMed: 15281071]
21. Ikeda K, Koenig JH. Morphological identification of the motor neurons innervating the dorsal longitudinal flight muscle of Drosophila melanogaster. The Journal of comparative neurology. 1988; 273(3):436–444. [PubMed: 3145293]
22. Trimarchi JR, Murphey RK. The shaking-B2 mutation disrupts electrical synapses in a flight circuit in adult Drosophila. J Neurosci. 1997; 17(12):4700–4710. [PubMed: 9169530]
23. van der Bliek AM, Meyerowitz EM. Dynamin-like protein encoded by the Drosophila shibire gene associated with vesicular traffic. Nature. 1991; 351(6325):411–414. [PubMed: 1674590]
24. Hinshaw JE, Schmid SL. Dynamin self assembles into rings suggesting a mechanism for coated vesicle budding. Nature. 1995; 374(6518):190–192. [PubMed: 7877694]
25. Sever S, Damke H, Schmid SL. Garrotes, springs, ratchets, and whips: putting dynamin models to the test. Traffic. 2000; 1(5):385–392. [PubMed: 11208124]
26. Kawasaki F, Hazen M, Ordway RW. Fast synaptic fatigue in shibire mutants reveals a rapid requirement for dynamin in synaptic vesicle membrane trafficking. Nat Neurosci. 2000; 3(9):859–860. [PubMed: 10966613]
27. Ramaswami M, Krishnan KS, Kelly RB. Intermediates in synaptic vesicle recycling revealed by optical imaging of Drosophila neuromuscular junctions. Neuron. 1994; 13(2):363–375. [PubMed: 8060617]
28. Poodry CA, Edgar L. Reversible alteration in the neuromuscular junctions of Drosophila melanogaster bearing a temperature-sensitive mutation, shibire. The Journal of cell biology. 1979; 81(3):520–527. [PubMed: 110817]

29. Koenig JH, Saito K, Ikeda K. Reversible control of synaptic transmission in a single gene mutant of Drosophila melanogaster. The Journal of cell biology. 1983; 96(6):1517–1522. [PubMed: 6304107]
30. Majumdar A, Ramagiri S, Rikhy R. Drosophila homologue of Eps15 is essential for synaptic vesicle recycling. Exp Cell Res. 2006; 312(12):2288–2298. [PubMed: 16709407]
31. Petrovich TZ, Merakovsky J, Kelly LE. A genetic analysis of the stoned locus and its interaction with dunce, shibire and Suppressor of stoned variants of Drosophila melanogaster. Genetics. 1993; 133(4):955–965. [PubMed: 8462853]
32. Kelly LE, Phillips AM. Molecular and genetic characterization of the interactions between the Drosophila stoned-B protein and DAP-160 (intersectin). The Biochemical journal. 2005; 388(Pt 1):195–204. [PubMed: 15631619]
33. Koh TW, Korolchuk VI, Wairkar YP, Jiao W, Evergren E, Pan H, Zhou Y, Venken KJ, Shupliakov O, Robinson IM, O'Kane CJ, Bellen HJ. Eps15 and Dap160 control synaptic vesicle membrane retrieval and synapse development. The Journal of cell biology. 2007; 178(2):309–322. [PubMed: 17620409]
34. Martina JA, Bonangelino CJ, Aguilar RC, Bonifacino JS. Stonin 2: an adaptor-like protein that interacts with components of the endocytic machinery. The Journal of cell biology. 2001; 153(5): 1111–1120. [PubMed: 11381094]
35. Rohrbough J, Broadie K. Lipid regulation of the synaptic vesicle cycle. Nat Rev Neurosci. 2005; 6(2):139–150. [PubMed: 15685219]
36. Yakir-Tamang L, Gerst JE. Phosphoinositides, exocytosis and polarity in yeast: all about actin? Trends Cell Biol. 2009; 19(12):677–684. [PubMed: 19818626]
37. Haucke V. Phosphoinositide regulation of clathrin-mediated endocytosis. Biochem Soc Trans. 2005; 33(Pt 6):1285–1289. [PubMed: 16246100]
38. Wenk MR, De Camilli P. Protein-lipid interactions and phosphoinositide metabolism in membrane traffic: insights from vesicle recycling in nerve terminals. Proc Natl Acad Sci U S A. 2004; 101(22):8262–8269. [PubMed: 15146067]
39. Leung HT, Tseng-Crank J, Kim E, Mahapatra C, Shino S, Zhou Y, An L, Doerge RW, Pak WL. DAG lipase activity is necessary for TRP channel regulation in Drosophila photoreceptors. Neuron. 2008; 58(6):884–896. [PubMed: 18579079]
40. Gronke S, Mildner A, Fellert S, Tennagels N, Petry S, Muller G, Jackle H, Kuhnlein RP. Brummer lipase is an evolutionary conserved fat storage regulator in Drosophila. Cell Metab. 2005; 1(5): 323–330. [PubMed: 16054079]
41. Vijayakrishnan N, Broadie K. Temperature sensitive paralytic mutants: insights into the synaptic vesicle cycle. Biochem Soc Trans. 2006; 34(Pt 1):81–87. [PubMed: 16417488]
42. Faulkner DL, Dockendorff TC, Jongens TA. Clonal analysis of cmp44E, which encodes a conserved putative transmembrane protein, indicates a requirement for cell viability in Drosophila. Dev Genet. 1998; 23(4):264–274. [PubMed: 9883579]
43. Shin BS, Maag D, Roll-Mecak A, Arefin MS, Burley SK, Lorsch JR, Dever TE. Uncoupling of initiation factor eIF5B/IF2 GTPase and translational activities by mutations that lower ribosome affinity. Cell. 2002; 111(7):1015–1025. [PubMed: 12507428]
44. Dellinger B, Felling R, Ordway RW. Genetic modifiers of the Drosophila NSF mutant, comatose, include a temperature-sensitive paralytic allele of the calcium channel alpha1-subunit gene, cacophony. Genetics. 2000; 155(1):203–211. [PubMed: 10790395]
45. Narayanan R, Leonard M, Song BD, Schmid SL, Ramaswami M. An internal GAP domain negatively regulates presynaptic dynamin in vivo: a two-step model for dynamin function. The Journal of cell biology. 2005; 169(1):117–126. [PubMed: 15824135]
46. Hojjati MR, van Woerden GM, Tyler WJ, Giese KP, Silva AJ, Pozzo-Miller L, Elgersma Y. Kinase activity is not required for alphaCaMKII-dependent presynaptic plasticity at CA3-CA1 synapses. Nat Neurosci. 2007; 10(9):1125–1127. [PubMed: 17660813]
47. McNiven MA, Cao H, Pitts KR, Yoon Y. The dynamin family of mechanoenzymes: pinching in new places. Trends Biochem Sci. 2000; 25(3):115–120. [PubMed: 10694881]
48. Orth JD, McNiven MA. Dynamin at the actin membrane interface. Curr Opin Cell Biol. 2003; 15(1):31–39. [PubMed: 12517701]

49. Sweitzer SM, Hinshaw JE. Dynamin undergoes a GTP-dependent conformational change causing vesiculation. Cell. 1998; 93(6):1021–1029. [PubMed: 9635431]
50. Stowell MH, Marks B, Wigge P, McMahon HT. Nucleotide-dependent conformational changes in dynamin: evidence for a mechanochemical molecular spring. Nat Cell Biol. 1999; 1(1):27–32. [PubMed: 10559860]
51. Grigliatti TA, Hall L, Rosenbluth R, Suzuki DT. Temperature-sensitive mutations in Drosophila melanogaster. XIV. A selection of immobile adults. Mol Gen Genet. 1973; 120(2):107–114. [PubMed: 4631264]
52. Chen MS, Obar RA, Schroeder CC, Austin TW, Poodry CA, Wadsworth SC, Vallee RB. Multiple forms of dynamin are encoded by shibire, a Drosophila gene involved in endocytosis. Nature. 1991; 351(6327):583–586. [PubMed: 1828536]
53. Koenig JH, Ikeda K. Synaptic vesicles have two distinct recycling pathways. The Journal of cell biology. 1996; 135(3):797–808. [PubMed: 8909551]
54. Zinsmaier KE, Eberle KK, Buchner E, Walter N, Benzer S. Paralysis and early death in cysteine string protein mutants of Drosophila. Science (New York, NY. 1994; 263(5149):977–980.
55. Dermaut B, Norga KK, Kania A, Verstreken P, Pan H, Zhou Y, Callaerts P, Bellen HJ. Aberrant lysosomal carbohydrate storage accompanies endocytic defects and neurodegeneration in Drosophila benchwarmer. J Cell Biol. 2005; 170(1):127–139. [PubMed: 15998804]

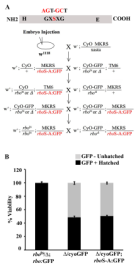

Figure 1. Lipase-domain *rbo* mutant fails to rescue *rbo* null mutant lethality

A, Schematic diagram showing the primary sequence of RBO with histidine (H) and glutamate (E) catalytic sites and the peptide motif of the serine active site. The serine was mutated to an alanine by substituting two nucleotides in the native gene shown above the protein structure. Below is shown the genetic scheme used to generate transgenic lines expressing lipase domain *rbo*S-A:GFP mutant in both *rbo* temperature sensitive (TS) and null mutant backgrounds. **B**, Quantification of embryo hatching to first instar larva viability in the three genotypes shown. GFP-negative embryos are null for *rbo*, due to the absence of the CyOGFP balancer. Bars show mean ± SD.

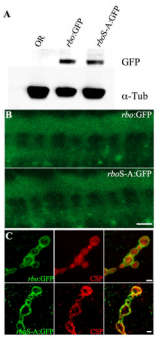

Figure 2. Lipase-domain mutant RBO protein is expressed normally

A, A representative Western blot showing *rbo*:GFP and *rbo*S-A:GFP protein from adult head extracts. α-Tubulin is the loading control. **B**, Representative images of *rbo*:GFP and *rbo*S-A:GFP in the stage 15 embryonic ventral nerve cord (VNC). Scale bar, 20μm. **C**, Representative images of *rbo*:GFP and *rbo*S-A:GFP in wandering 3rd instar neuromuscular junction (NMJ) boutons. Co-labeled with the presynaptic marker cysteine string protein (CSP). Scale bar, 2μm.

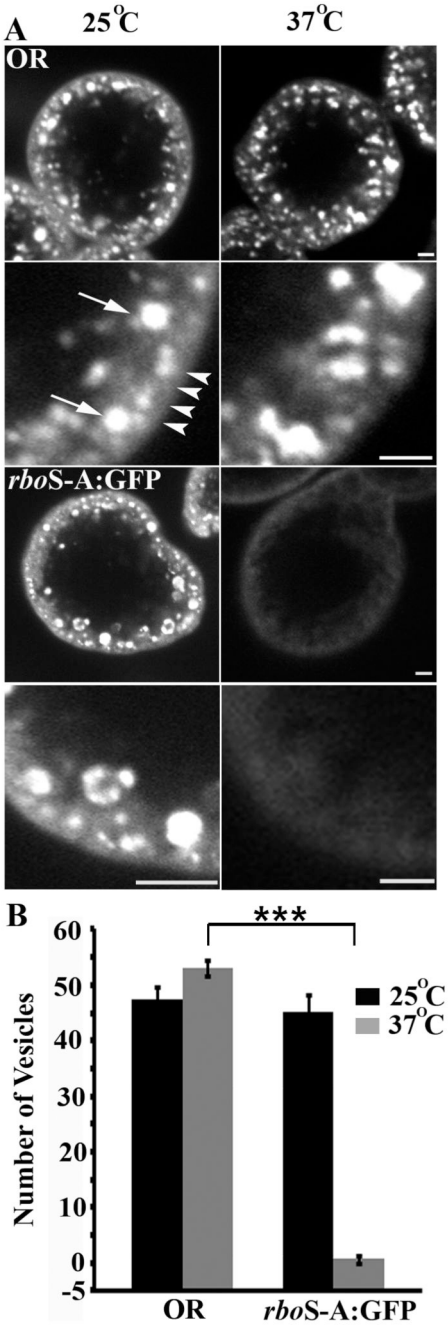

Figure 3. Lipase-domain *rbo* mutant fails to rescue *rbo*^{ts} Garland cell endocytosis

A, Representative images showing texas-red avidin uptake in Garland cells of indicated genotypes loaded at permissive (25°C) and restrictive (37°C) temperatures. Lower panels in each case show higher magnification of the region just below the plasma membrane. White arrows point to vesicles and arrowheads point to plasma membrane. Scale bar, 2 μm. **B**, Quantification of the number of texas-red avidin positive vesicles in wildtype control (OR) and lipase-domain *rbo* mutant (*rbo*S-A:GFP) with permissive and restrictive temperature loading. The bars show the mean ± SEM. Significance of $p<0.001$ is indicated (***).

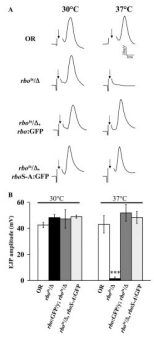

Figure 4. Lipase-domain *rbo* mutant rescues *rbo*^{ts} synaptic transmission

A, Representative excitatory junctional potential (EJP) recordings from the adult DLM. The arrow indicates initiation of the evoked shock artifact that was removed for clarity. The four genotypes are wildtype control (OR), conditional *rbo* mutant (*rbo*^{ts}/Δ), *rbo*^{ts}/Δ expressing wildtype *rbo:*GFP and *rbo*^{ts}/Δ expressing mutant *rbo*S-A:GFP. Records are shown at permissive 30°C (left) and restrictive 37°C (right). **B**, Quantification of mean EJP amplitudes in all four genotypes at 30°C and after 5 minutes at 37°C. The bars show the mean ± SEM. Significance of $p<0.001$ is indicated (***).

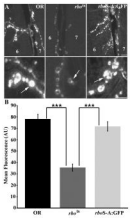

Figure 5. Lipase-domain *rbo* mutant rescues *rbo*^{ts} NMJ synaptic endocytic defect

A, Representative images of 3rd instar larval NMJ terminals in control (OR), *rbo*^{ts} and *rbo*^{ts}; *rbo*S-A:GFP animals loaded with FM1–43 dye at 37°C. Scale bar, 2μm. Lower panels show higher magnification view of synaptic boutons from the terminals shown above. Scale bar, 1μm. **B**, Quantification of FM1–43 dye loading. The presence of *rbo*S-A:GFP in the *rbo*^{ts} background fully rescues the endocytic defect seen in *rbo*^{ts} at restrictive temperature. Significance of $p<0.001$ is indicated (***).

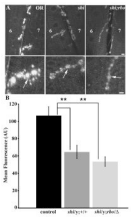

Figure 6. Interaction of RBO with Dynamin dependent endocytosis at the NMJ

A, Representative images showing FM1–43 dye loading in 3rd instar larval NMJs loaded in depolarizing saline for 4 minutes at 18°C. Scale bar, 2μm. Lower panels show higher magnification of synaptic boutons from terminals in above panels. Scale bar, 1μm. **B**, Quantification of FM1–43 dye loading showing relative dye loading intensity between OR, *shi*^{ts1}/y, and *shi*^{ts1}/y; *rbo*^{ts}/Δ genotypes. Significance of $p<0.01$ is indicated (**).

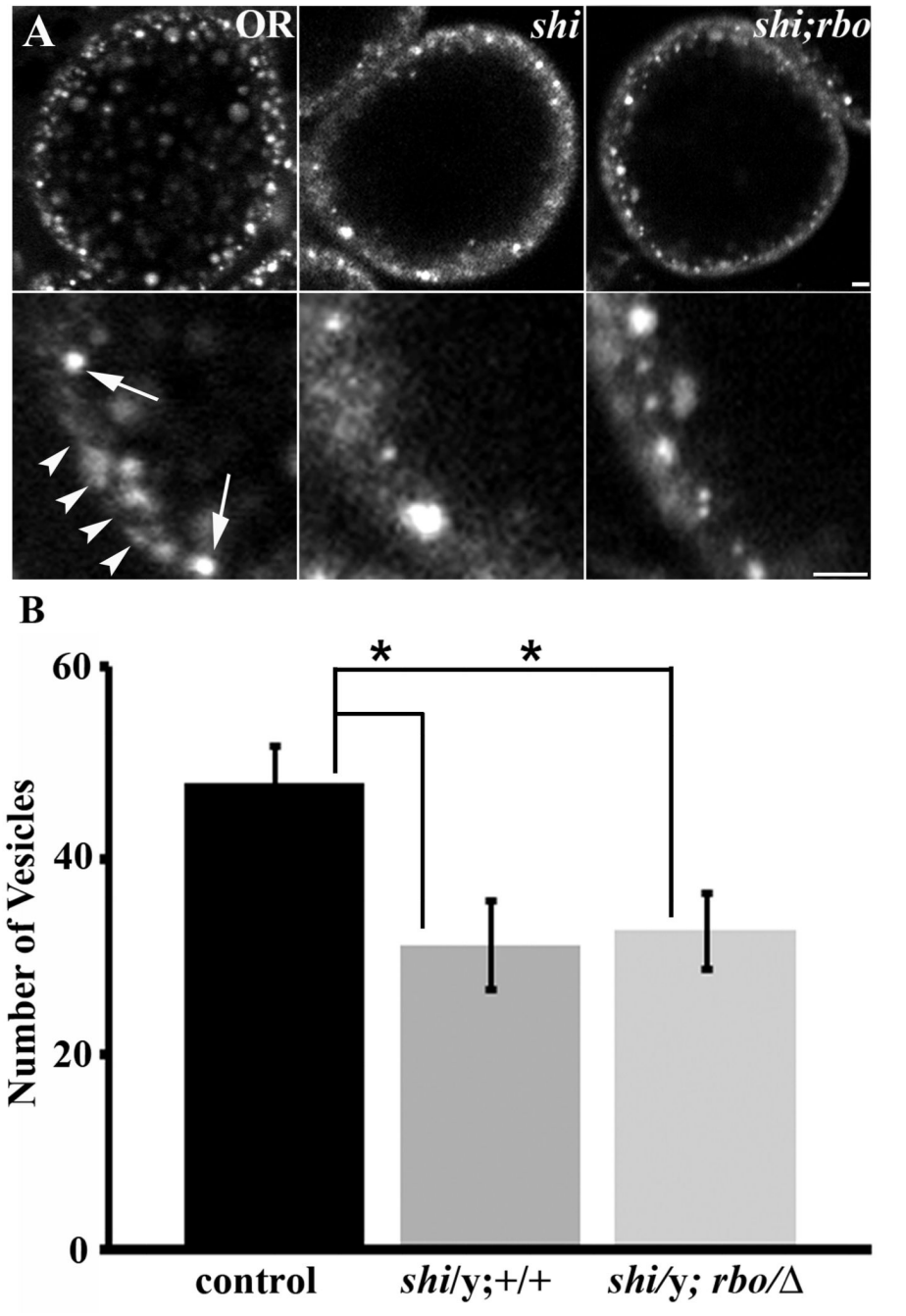

Figure 7. RBO interaction with Dynamin dependent endocytosis in Garland cells

A, Representative images showing texas-red avidin uptake in Garland cells of *shi*^{ts1}/y, and *shi*^{ts1}/y;*rbo*/Δ larvae loaded at 18°C for 5 minutes. Scale bar, 5μm. Lower panels show higher magnification view of Garland cell plasma membrane from cells shown in upper panel. Scale bar, 2.5μm. **B**, Quantification of Garland cell endocytosis by counting number of fluorescent punctae. Significance of $p<0.05$ is indicated (*).

Table 1

Time to reach TS paralysis (%)

	Time (min:sec)				
35°C	**6**	**7**	**8**	**9**	**10**
OR	0	0	0	0	0
rbo^{ts}/*Δ*	7±4	13±8	50±9	80±5	100
rbo^{ts}*Δ*/ with *rbo*:GFP	0	0	0	0	0
rbo^{ts}*Δ*/ with *rbo*:S-A:GFP	0	0	0	0	0
37°C	**1**	**2**	**3**	**4**	**5**
OR	0	0	0	0	0
rbo^{ts}/*Δ*	0	0	57±8	83±6	100
rbo^{ts}/*Δ* with *rbo*:GFP	0	0	0	0	0
rbo^{ts}/*Δ* with *rbo*:S-A:GFP	0	0	0	0	0
39°C	**1**	**1:30**	**2**	**2:30**	**3**
OR	0	0	0	0	0
rbo^{ts}/*Δ*	0	14±8	43±10	86±4	100
rbo^{ts}/*Δ* with *rbo*:GFP	0	0	0	0	0
rbo^{ts}/*Δ* with *rbo*:S-A:GFP	0	0	0	0	0

The table shows the amount of time (in min:sec) it takes for each genotype (left column) to paralyze (percent paralyzed ± SEM). Temperatures tested include 35°C, 37°C and 39°C. Paralysis is defined as complete cessation of all movement.

Table 2

Time to reach TS paralysis (%)

	Time (min:sec)				
35°C	**6**	**7**	**8**	**9**	**10**
rbo^{ts}/*Δ*	7±4	13±8	50±9	80±5	100
eps15$^{\Delta}$,*rbo*^{ts}/*Δ*	7±4	17±11	43±11	83±6	100
stn^{PH1}/FM7; *rbo*^{ts}/*Δ*	10±6	25±10	55±5	80±8	100
stn$^{13-120}$/FM7; *rbo*^{ts}/*Δ*	10±6	20±8	55±5	70±6	100
37°C	**1**	**2**	**3**	**4**	**5**
rbo^{ts}/*Δ*	0	0	57±8	83±6	100
eps15$^{\Delta}$,*rbo*^{ts}/*Δ*	0	3±3	50±4	90±4	100
stn^{PH1}/FM7; *rbo*^{ts}/*Δ*	0	3±3	50±4	77±3	100
stn$^{13-120}$/FM7; *rbo*^{ts}/*Δ*	0	5±5	30±10	75±5	100
39°C	**1**	**1:30**	**2**	**2:30**	**3**
rbo^{ts}/*rbo*$^{\Delta}$	0	14±8	43±10	86±4	100
eps15$^{\Delta}$,*rbo*^{ts}/*Δ*	0	17±7	43±9	74±6	100
stn^{PH1}/FM7; *rbo*^{ts}/*Δ*	0	10±6	45±10	75±5	95±5
stn$^{13-120}$/FM7; *rbo*^{ts}/*Δ*	0	15±10	40±8	80±0	100

The table shows the amount of time (in min:sec) it takes for each genotype (left column) to paralyze (percent paralyzed ± SEM). Temperatures tested include 35°C, 37°C and 39°C. Paralysis is defined as complete cessation of all movement.